Fatigue stress spectra and reliability evaluation of short- to medium-span bridges under stochastic and dynamic traffic load

Donghuang Yan[1]; Yuan Luo[2]; Naiwei Lu[3]; Ming Yuan[4]; Michael Beer[5]

Abstract:

This study presents a novel approach to simulating the fatigue stress spectra of short- to medium-span bridges under stochastic and dynamic traffic loads. The stochastic traffic load is simulated based on the weigh-in-motion (WIM) measurements of a heavy-duty highway bridge in China, and the dynamic effects are modeled using a vehicle-bridge coupled vibration system. An interpolation response surface method (RSM) is used to approximate the effective stress ranges of a bridge with respect to road roughness conditions, gross vehicle weights, vehicle configurations, and driving speeds. The RSM provides a platform for an efficient spectrum simulation of bridges under stochastic and dynamic traffic loads. A case study of a simply supported T-girder bridge demonstrates the effectiveness and efficiency of the proposed approach. The proposed computational framework provides an effective approach for simulating the fatigue stress spectra for short-to medium-span bridges with WIM data.

[1] Professor, School of Civil Engineering and Architecture, Changsha Univ. of Science and Technology, Changsha Hunan 410114, China. Email: yandonghuang@126.com

[2] Research assistant, School of Civil Engineering and Architecture, Changsha Univ. of Science and Technology, Changsha Hunan 410114, China. Email: luoyuanbridge@163.com

[3] Lecturer, School of Civil Engineering and Architecture, Changsha Univ. of Science and Technology, Changsha Hunan 410114, China. Email: lunaiweide@163.com

[4] Assistant Prof., School of Civil Engineering and Architecture, Changsha Univ. of Science and Technology, Changsha Hunan 410114, China. Email: yuanming_dt@163.com

[5] Professor, Institute for Risk and Relide@ability, Leibniz Universität Hannover, Hannover 31509, Germany. Email: beer@irz.uni-hannover.de

However, the efficiency of the approach depends on the number of intervals of driving speed and gross vehicle weight in the interpolation RSM. Additionally, overloading control has a considerable influence on the probability density of the high-amplitude stresses in the fatigue stress spectrum. Even a relatively high overloading limit value will considerably increase the fatigue reliability of a bridge. In addition, the numerical results provide a theoretical basis for bridge deck retrofitting and truck overloading control measures.

Keywords: fatigue stress spectrum; fatigue reliability; vehicle-bridge interaction; response surface method; stochastic traffic load; weigh-in-motion; road roughness condition

Introduction

Due to the steady development of the global economy and national transportation industries, traffic loading has significantly increased in recent decades (Capros et al. 2008). The traffic growth has occurred not only in traffic volume, but also in the number of extremely overloaded trucks (Mei et al. 2004; Han et al. 2014). This phenomenon negatively influences existing bridges, via large maximum traffic load effects (Obeirn and Enright 2013; Lu et al. 2017), exponential increases in fatigue damage (Theil 2016), and road roughness deterioration (Pais et al. 2013). Research progress has been made on the fatigue life and serviceability evaluation of existing steel and concrete bridges (Wang et al. 2015; Lu et al. 2017). For short-to medium-span bridges, deteriorating road roughness conditions (RRCs) can lead to more stress cycles and high stress amplitudes due to dynamic impacts (Zhang and Cai 2012). A low dead-to-live load ratio (Deng and Cai 2010a) is another characteristic of short-to medium-span bridges highlighting the importance of considering actual traffic loads in fatigue safety assessments. In practice, some researchers (Mohammadi and Polepeddi 2000; Wang et al.

2016b) have noted that the current practice of bridge fatigue design codes may underestimate the dynamic effects and the fatigue stress spectrum of some in-service bridges. Therefore, a bridge fatigue evaluation accounting for dynamic effects and actual traffic loads deserves investigation.

Fatigue stress spectra are essential for fatigue reliability evaluations and fatigue life prediction for existing bridges. Since the stress spectrum is sensitive to site-specific traffic loads, a numerical simulation based on weigh-in-motion (WIM) measurements is an effective method for simulating the stress spectra for an extensive range of bridges, in addition to the structural health monitoring (SHM) approach (Chen et al. 2012; Deng et al. 2015). In this regard, numerous studies have been conducted to develop fatigue truck-load models based on site-specific WIM measurements (Wang et al. 2005; Chen et al. 2015). Compared with standard fatigue truck-load models with deterministic configurations and gross vehicle weights (GVWs), stochastic traffic load models with uncertainties associated with individual vehicles or traffic flows on a bridge are more effective for the stress spectrum simulation. A probabilistic finite element method (FEM) was developed by Guo et al. (2012) to evaluate the fatigue reliability of a steel bridge based on WIM measurements. Fatigue stress spectra of welded joints in orthotropic steel bridge decks were evaluated by Lu et al. (2016), who utilized stochastic fatigue truck-load models and learning machines. These studies focused on the fatigue stress spectrum simulation of bridges based on site-specific WIM measurements. However, the dynamic impacts of the traffic load, which are greater for short-to medium-span bridges with poor RRCs, were not considered in their investigations. In addition to the stress amplification, the number of stress cycles also increase due to the vehicle-bridge interaction

(VBI). Wang et al (2016a) indicated that the number of stress cycles used in current studies for short-span concrete bridges may be overestimate. However, Lee et al. (2012) showed that the fatigue dynamic factor for steel plate girder railway may be overestimated.

National design codes (BIS 2006; AASHTO 2012) have recommended using dynamic amplification factors (DAFs) to describe the dynamic effects on short-to medium-span bridges. However, the vehicle-induced dynamic effects on bridge fatigue damage are not covered in the conventional DAFs. Low-amplitude stress cycles due to VBIs contribute to fatigue damage accumulation. Therefore, VBI analysis is essential for the fatigue stress analysis of short-to medium-span bridges. Deng and Cai (2010a) highlighted the influence of RRC deterioration of a short-span bridge on the DAFs, and suggested a modification to the AASHTO specifications. Wang et al. (2016b) evaluated DAFs for the fatigue design of steel I-girder bridges by considering the deterioration of RRCs and investigated the influence of the dynamic effects of overloaded vehicles on the fatigue stress. These studies emphasize the influence of RRCs and truck overloading on dynamic impacts and DAFs. However, the above studies estimated DAFs mainly through analyzing an AASHTO HS 20-44 truck, but this process does not comprehensively describe the characteristics of the actual traffic load. In addition, to the best of the author’s knowledge, few studies have introduced VBI analysis into the fatigue stress spectrum simulation, especially under stochastic traffic loads.

This study aims to develop a computational framework for the fatigue stress spectrum simulation of short-to medium-span bridges considering stochastic and dynamic traffic loads. The stochastic traffic load is simulated based on WIM measurements of a heavy-duty highway bridge in China, and the dynamic effects are modeled via a vehicle-bridge coupled vibration

system. An interpolation response surface method is utilized to efficiently evaluate the stress spectrum. The bridge effective stress ranges are evaluated considering RRCs, GVWs, vehicle speeds, and vehicle configurations. The efficiency of the approach and its application to fatigue reliability assessment are demonstrated by a case study of a simply supported T-girder bridge.

Theoretical bases

Vehicle-bridge coupled system

A vehicle-bridge coupled system is a dynamic system composed of moving vehicles, bridge structures and RRCs. The bridge deflection and the RRCs cause the vibration in the VBIs, which couple the vibration of both the bridge and the vehicle. In a vehicle-bridge coupled system, both the bridge and the vehicle are usually simulated as discrete systems when constructing their equations of motion. The two systems are coupled with assumptions of the same displacement and interaction at the contact points (Wang et al. 2016a). A vehicle can be simulated as the vehicle body, vehicle tires and suspension. For instance, a two-axle truck is usually modeled as a four degree-of-freedom (DOF) system, including sinking and rotation of the truck body and the vertical displacements of the front and rear tires, as shown in **Fig. 1**. The equation of motion of a vehicle-bridge coupled system is written as follows (Zhang and Cai 2012):

$$\begin{bmatrix} \mathbf{M}_b & \\ & \mathbf{M}_v \end{bmatrix} \begin{Bmatrix} \ddot{\mathbf{u}}_b \\ \ddot{\mathbf{u}}_v \end{Bmatrix} + \begin{bmatrix} \mathbf{C}_b + \mathbf{C}_{bb} & \mathbf{C}_{bv} \\ \mathbf{C}_{vb} & \mathbf{C}_v \end{bmatrix} \begin{Bmatrix} \dot{\mathbf{u}}_b \\ \dot{\mathbf{u}}_v \end{Bmatrix} + \begin{bmatrix} \mathbf{K}_b + \mathbf{K}_{bb} & \mathbf{K}_{bv} \\ \mathbf{K}_{vb} & \mathbf{K}_v \end{bmatrix} \begin{Bmatrix} \mathbf{u}_b \\ \mathbf{u}_v \end{Bmatrix} = \begin{Bmatrix} \mathbf{F}_{br} \\ \mathbf{F}_{vr} + \mathbf{F}_V^G \end{Bmatrix} \quad (1)$$

where $\mathbf{M}_v$, $\mathbf{C}_v$, and $\mathbf{K}_v$ are the mass, the damping and the stiffness matrices of the vehicle, respectively; $\mathbf{M}_b$, $\mathbf{C}_b$ and $\mathbf{K}_b$ are the mass, the damping and the stiffness matrices of the bridge, respectively; $\mathbf{u}_v$ and $\mathbf{u}_b$ are the displacement vectors of the vehicle and the bridge, respectively;

and $\mathbf{C}_{bb}$, $\mathbf{C}_{bv}$, $\mathbf{C}_{vb}$, $\mathbf{K}_{\mathrm{bb}}$, $\mathbf{K}_{bv}$, $\mathbf{K}_{vb}$, $\mathbf{F}_{br}$ and $\mathbf{F}_{vr}$ are additional terms related to the expansion of the wheel-road contact force. These time-variant parameters will change as the vehicle moves across the bridge.

For short-to medium-span bridges, the bridge behavior can be modeled linearly, which enables the use of the modal superposition to reduce the number of DOFs in a system. It is acknowledged that $\{\Phi_i\}^{\mathrm{T}}[\mathbf{M}_{\mathrm{b}}]\{\Phi_i\}=1$, $\{\Phi_i\}^{\mathrm{T}}[\mathbf{K}_{\mathrm{b}}]\{\Phi_i\}=\omega_i^2$ and $[\mathbf{C}_{\mathrm{b}}]=2\omega_i\eta_i[\mathbf{M}_{\mathrm{b}}]$, where ω_i is the frequency of the ith mode shape of the bridge and η_i is the percentage of the critical damping for the ith mode of the bridge. Therefore, **Eq. (1)** can be written in the frequency domain:

$$\begin{bmatrix}\mathbf{I} & \\ & \mathbf{M}_v\end{bmatrix}\begin{Bmatrix}\ddot{\boldsymbol{\xi}}_b \\ \ddot{\mathbf{u}}_v\end{Bmatrix}+\begin{bmatrix}2\omega_i\eta_i\mathbf{I}+\boldsymbol{\Phi}_b^T\mathbf{C}_{bv} & \Phi_b^T\mathbf{C}_{bv} \\ \mathbf{C}_{vb}\boldsymbol{\Phi}_b & \mathbf{C}_v\end{bmatrix}\begin{Bmatrix}\dot{\boldsymbol{\xi}}_b \\ \dot{\mathbf{u}}_v\end{Bmatrix}$$
$$+\begin{bmatrix}\boldsymbol{\omega}_i^2\mathbf{I}+\boldsymbol{\Phi}_b^T\mathbf{K}_{bb}\boldsymbol{\Phi}_b & \boldsymbol{\Phi}_b^T\mathbf{K}_{bv} \\ \mathbf{K}_{vb} & \mathbf{K}_v\end{bmatrix}\begin{Bmatrix}\boldsymbol{\xi}_b \\ \mathbf{u}_v\end{Bmatrix}=\begin{Bmatrix}\boldsymbol{\Phi}_b^T\mathbf{F}_{br} \\ \mathbf{F}_{vr}+\mathbf{F}_V^G\end{Bmatrix} \tag{2}$$

where $\mathbf{I}$ is a unit matrix, ξ_b is the generalized coordinate vector of the bridge, and the bridge deflection vector can be written by the superposition $\mathbf{u}_b=[\Phi_b]\{\xi_b\}$. Based on the deflection-strain relationship and the stress-strain relationship, the stress can be written as follows:

$$\mathbf{S}=\mathbf{EBu}_b \tag{3}$$

where $\mathbf{S}$ is the estimated stress vector; $\mathbf{E}$ is the stress-strain relationship matrix, which can be assumed to be a constant; and $\mathbf{B}$ is the stress-deflection relationship matrix, which can be deduced from the element shape function.

In summary, the equations of motion of the bridge and the vehicle are modeled separately and are then coupled together at the point of contact in terms of deflection and interaction. With

123 modal parameters extracted from a bridge finite element model, the deflection vector can be
124 evaluated based on Eq. 2. Finally, the rebar stress can be calculated based on the
125 strain-displacement and stress-strain relationship from the finite element model and elastic
126 mechanics theories. Note that the friction and the slip between the rebar and the concrete are not
127 considered, because the focus of the present study was on the traffic patterns.

128 ***Fatigue damage accumulation***

129 The stress blocks computed based on the vehicle-bridge coupled system can be converted into
130 fatigue damage using S-N (stress-life) curves. The traffic-induced stress cycles are mostly
131 high-cycle and low-amplitude blocks. Therefore, Eurocode3 (ECS 2005), as one of the national
132 fatigue design codes, was used to the define S-N curves, due to its consideration of a special
133 slope value for the low-amplitude stress cycles and detailed categories. The S-N curves in
134 Eurocode3 are written as follows:

135 $$\Delta\sigma^3{}_R N_R = K_C \quad (K_C = 2\times10^6 \Delta\sigma^3{}_C \quad \Delta\sigma_R \geq \Delta\sigma_D) \tag{4}$$

136 $$\Delta\sigma^5{}_R N_R = K_D \quad (K_D = 5\times10^6 \Delta\sigma^5{}_C \quad \Delta\sigma_L < \Delta\sigma_R \leq \Delta\sigma_D) \tag{5}$$

137 where $\Delta\sigma_R$ is the stress range; N_R is the corresponding number of cycles; $\Delta\sigma_D$ and $\Delta\sigma_L$ are the
138 constant-amplitude fatigue limit and the fatigue threshold, respectively; and K_C and K_D are the
139 fatigue strength coefficients when $\Delta\sigma_R>\Delta\sigma_D$ and $\Delta\sigma_L<\Delta\sigma_R\leq\Delta\sigma_D$, respectively. For concrete
140 bridges, the fatigue critical components are usually the longitudinal rebars in the bottom of the
141 girder section. The specific category of rebar is the butted joint in Eurocode3, and the
142 parameters in the S-N curve are shown in **Table 1**.

143 Notably, the vehicle-induced vibration yields numerous variable-amplitude stress blocks
144 that can be equivalent to a constant-amplitude stress block with the same fatigue damage.

Although the low-amplitude stresses included in the variable-amplitude stress blocks are usually lower than the fatigue threshold (32MPa), they cannot be cut off (Chan et al. 2001). Therefore, the stress fatigue threshold of $\Delta\sigma_L$=0 MPa was considered in the present study to make the estimation more realistic. Based on the S-N curves and Palmgren linear fatigue damage accumulation rule (Miner 1945), the equivalent formulation can be written as follows:

$$\Delta\sigma_{re}^5 = \frac{\sum \frac{N_i \Delta\sigma_i^3}{K_C} + \sum \frac{N_j \Delta\sigma_j^5}{K_D}}{\left(\sum N_i + \sum N_j\right) / K_D} \tag{6}$$

where $\Delta\sigma_i$ and $\Delta\sigma_j$ are the ith and jth stress ranges that are larger than $\Delta\sigma_D$ and less than $\Delta\sigma_D$, respectively; N_i and N_j are the number of cycles with respect to $\Delta\sigma_i$ and $\Delta\sigma_j$, respectively; and $\Delta\sigma_{re}$ is the equivalent efficient stress range. Note that the stress limit was not considered in the present study. Herein, the fatigue stress and fatigue damage accumulation due to the passage of an individual truck on a bridge can be evaluated by considering the VBI.

By expanding the individual vehicle effect to the traffic effect, the fatigue stress spectra of a bridge can be simulated and applied in fatigue life prediction and fatigue reliability assessment. A structural limit state function (LSF), which is composed of stochastic parameters in terms of the resistance and the load effect, is essential for fatigue reliability evaluation. A positive LSF value indicates the fatigue safety of a bridge, whereas a negative value indicates the fatigue failure of a bridge. In addition to the stress spectrum and the structural resistance parameters, the average daily truck traffic (ADTT) is another critical parameter associated with numerous factors, including the local economy and governmental policies. This study assumes that the annual ADTT increases linearly. Based on the this assumption, the LSF of the fatigue damage accumulation during the lifetime of a bridge is written as follows:

$$g_n(X) = D_\Delta - D_n(\mathrm{X}) = D_\Delta - 365\Delta\sigma_{re}^5 N_d e \cdot \sum_{t=1}^{n}\left[1+(t-1)R_{ADTT}\right] / K_D \quad (7)$$

where $g_n(X)$ is the LSF of a bridge in the nth year, X is a random variable vector, D_Δ is the Miner's critical fatigue damage index, $D_n(X)$ is the cumulative fatigue damage in the nth year, e is the distribution coefficient of the transverse axle load, N_d is the number of daily cycles that correspond to $\Delta\sigma_{re}$, and R_{ADTT} is the annual linear growth factor of the daily traffic volume. The most critical random variables in **Eq. (7)**, which are associated with traffic load, are the equivalent stress ranges and the corresponding number of stress cycles. In this study, the probability models of the two random variables are evaluated from WIM measurements based on an efficient approach described below. Eventually, the fatigue reliability of the LSF can be evaluated using the conventional first-order second-moment method or a Monte Carlo simulation (MCS).

An efficient approach for bridge dynamic stress spectrum simulation based on WIM measurements

Review of conventional approaches

Fatigue spectra are essential for the fatigue damage evaluation of bridges. The fatigue life prediction of bridges would be significantly affected by slight errors in the stress spectrum simulation. Fatigue stress spectra can be measured via bridge field tests, such as conventional bridge detection and the SHM approach (Liu et al. 2010; Ye et al. 2012; Soliman et al. 2015). Field tests can provide practical stress spectra based on continuously field-measured dynamic strain data. However, a relatively short time period of monitoring is hardly able to represent the fatigue stresses over the lifetime of a bridge. In addition, the expensive sensors and environmentally sensitive characteristics complicate the application of SHM.

188 In addition to the conventional monitoring approaches, numerical simulation represent an
189 alternative approach for fatigue stress analysis. The integration of a static influence line and
190 DAFs is a reliable approach recommended in several design specifications. However, the
191 DAFs might underestimate the dynamic effects, especially association with RRC deterioration.
192 Chan et al. (2003) calculated the fatigue stress of components of the Tsing Ma Bridge using a
193 loading moving force on the bridge. Zhou et al. (2013) obtained the fatigue stress of the Sesia
194 Bridge and identified the critical fatigue members by simplifying a high-speed train into a
195 series of concentrated forces. However, the existence of fatigue damage induced by the local
196 vibration of components highlighted the significance of introducing VBIs into the fatigue stress
197 evaluation. In recent decades, extensive studies have focused on vehicle-bridge coupled
198 vibration using various analytical models. With the application of these theoretical models, the
199 displacement, acceleration and dynamic stress response of bridges can be adequately simulated.
200 Deng and Cai (2010a) utilized a 3-D VBI model to evaluate the DAFs for short-span bridges.
201 Wang and Deng. (2015; 2016a) proposed simple and reasonable expressions for DAFs of the
202 stress ranges and the number of stress cycles for fatigue design. Zhang and Cai (2012)
203 evaluated the fatigue reliability of existing bridges based on the vehicle speed and the RRCs
204 via vehicle-bridge coupled vibration analysis. However, the truck load model in design
205 specifications might underestimate the vehicle load effects (Wang et al. 2016b).

206 In summary, most research efforts on fatigue stress spectrum simulation of bridges based
207 on WIM measurements have ignored the dynamic impact effect, which is more important for
208 short-to medium-span bridges. However, studies on the dynamic impact effect caused by
209 vehicle-bridge coupled vibration have mainly focused on amending the DAFs, while the

application of the dynamic impact effect in the stress spectrum simulation has been relatively limited. For more reasonable stress spectra, in addition to the vehicle-bridge coupled vibration analysis, the stochastic effects on bridges based on actual traffic loads should be considered. However, one of the challenges for considering both dynamic and stochastic effects is the time-consuming computational effort associated with the combined utilization of mode superposition and successive integration methods.

Computational framework for fatigue stress spectrum simulation

Based on the theoretical bases and discussions illustrated above, this study presents an efficient approach to simulate fatigue stress spectrum of short-to medium-span bridges. This approach incorporates both the stochastic traffic load and the VBI theory. An interpolation response surface method (RSM) is presented to make the stress spectra simulation more efficient. A flowchart of the computational framework is shown in **Fig. 2**. As depicted in **Fig. 2**, the procedures on the left side describe the simulation of individual trucks and traffic flows based on WIM measurements, while the procedures on the right side are associated with the VBI analysis. These procedures are described further below.

With WIM measurements, the first task is to classify the vehicles. The principle of the classification in this study is the axle configuration, where vehicles with the same or similar axle configurations are classified as a single type. Following the classification of vehicle types, the subsequent step is the probability modeling of the GVWs and the driving speeds of each vehicle type. The GVW intervals and the driving speed intervals will be used for the bridge time-stress history simulation. With the statistical model obtained from the WIM measurements, the stochastic traffic load model can be simulated via an MCS. Finally, the long-term traffic

load models will be used for bridge fatigue stress analysis.

The right side of the flowchart starts with the bridge model shapes and mode frequencies, which can be obtained from the finite-element model. With the individual truck intervals and RRCs, a VBI system is established. Bridge stress histories can be obtained via the equation of motion of the coupled system, as shown in **Eq. (2)**, by using the Newmark-β intergration approach. The stress history is simulated step-by-step with truck interval samples. Subsequently, variable-amplitude stress cycles in the stress histories can be counted via the rain-flow counting method. These variable-amplitude stress cycles under individual vehicle loads are converted to an efficient constant-amplitude stress cycle with the same fatigue damage. The GVWs and the driving speeds are both continuous, but the RRCs and vehicle types are discrete. Therefore, the response surface functions of the effective stress ranges for different RRCs and vehicle types are independent. The response surface functions affected by the GVW and the driving speed can be approximated by linear interpolation functions. Since the influence of the vehicle speed on the bridge dynamic amplification effect is not monotonic, the linear interpolation function is utilized. Therefore, the width of the driving speed intervals is a critical factor affecting the computational efficiency and the accuracy.

As elaborated above, the critical procedure of the framework is to utilize response surface functions to predict the stress ranges due to stochastic vehicle loads. The response surface function is approximated for several sample vehicles by taking the GVW and the vehicle speed as input data and the equivalent stress range as output data. The stochastic traffic load model is simulated with site-specific WIM measurements. The advantage of this framework is its ability to solve the time-consuming process associated with calculating the integral of the

vehicle-bridge coupled vibration.

Stress spectrum simulation of simply supported bridges

Stochastic traffic load simulation based on WIM measurements

A WIM system is composed of a set of sensors and support equipment to measure the emergence and the weight of passing vehicles. It is an effective management tool for truck overload control. A technical problem of the WIM system involves ensuring the weighing accuracy under environment interference. The wavelet decomposition method and the reconstruction method (Chatterjeed et al. 2006) are effective in this regard. The present study used the WIM data collected from a highway bridge in Sichuan Province, China. Details of the relevant data can be found in Liu et al. (2015). Note that the WIM system directly provided the relevant WIM data, including the vehicle type, the driving speed, the headway time, and the weight.

Statistical analysis and filtering processes were conducted to remove invalid data. The criteria for identifying invalid data are as follows: (1) the GVW is less than 30 kN; (2) the axle weight is greater than 300 kN or less than 5 kN; and (3) the vehicle length is greater than 20 m or less than 3 m. The effective data were classified into 6 categories according to the axle configuration, where V1 represents light cars and V2 to V6 represent two- to six- axle trucks. Taking a six-axle truck as an example, the probability density functions (PDFs) of the GVW and the driving speed are shown in **Fig. 3**. As shown in **Fig. 3**, heavy trucks present a relatively high proportion and have a high overload ratio in the PDF of GVWs. Based on these statistics, the stochastic traffic load in the slow lane was simulated via the MCS, as shown in **Fig. 4**.

In **Fig. 4**, each truck is stochastic but they follow the corresponding distribution. Using

this method, the stochastic traffic load has been simulated. The statistical vehicle parameters, including the vehicle type, the vehicle speed and the GVW, provide a basis for the subsequent dynamic analysis.

Fatigue stress simulation of simply supported bridges

Two simply supported T-girder prestressed concrete (PC) bridges with span lengths of 25 m and 40 m are chosen here as examples to demonstrate the application of the proposed methodology. The dimensions of the cross-sections of the bridges are shown in **Fig. 5**. The fatigue-critical components of the bridges are the longitudinal steel bars at the bottom of the T-girder. The physical properties of the T-girder are shown in **Table 2**, where L_b is the span length of the girder; H_b is the height of the T-girder; A_c and A_s are the cross-sectional areas of a girder and a critical rebar, respectively; E is the modulus of elasticity of the rebar; I is the inertia moment of the girder; and y is the distance between the centroid of the cross-section to the critical steel bar. Mode shapes and mode frequencies were extracted from a 3D finite element model. The first-order mode shapes for both bridges are symmetric vertical bending, and the corresponding first natural frequencies for the 25-m-span and 40-m-span bridges are 4.99 Hz and 3.33 Hz, respectively.

According to the framework shown in **Fig. 2**, the subsequent procedure is to simulate the stress history of the critical rebar under an individual vehicle load. The RRC has a significant influence on the VBI, and is usually simulated by an inverse Fourier transformation and an assumed power spectral density. The RRC coefficients were simulated in the time domain as shown in **Fig. 6**, where the RRC coefficients for “Good” and “Poor” are 32×10^{-6} and 512×10^{-6} m^3/cycle, respectively.

Initially, a six-axle truck with a GVW of 550 kN was assumed to pass over the bridge with a constant speed of 15 m/s. Based on the VBI analysis, the dynamic stresses of the bottom steel bar of the #2 girder were evaluated by considering good and poor RRCs, respectively. The stress histories are shown in **Fig. 7**, where L_{v6} is the length of the six-axle truck, $\Delta\sigma_{re,s}$ is the static equivalent stress range, and $\Delta\sigma_{re,g}$ and $\Delta\sigma_{re,p}$ are the dynamic equivalent stress ranges for the good and poor RRCs, respectively. The stress ranges were calculated based on **Eq. (6)** and the S-N curve shown in Table 1. The equivalent stress ranges are obviously greater than the maximum stresses due to the additional stress cycles.

The DAFs and fatigue damage ratio between the DAFs of the $\Delta\sigma_{re}$ and the code are evaluated as shown in Table 3. The fatigue damage of a 25-m-span bridge with a poor RRC is 1.87 times greater than the one evaluated from the MOCAT specifications (2015). This result demonstrates the significance of accounting for the RRC effects in a VBI system when evaluating vehicle-induced fatigue damage. Since the bridge girder with L_b = 40 m has a higher fatigue stress range, this study will focus on the stress spectrum and reliability evaluation of the 40-m-span PC T-girder bridge.

Response surface function

As depicted in **Fig. 2**, the GVW, vehicle type and driving speed are considered in the VBI analysis. First, the GVW and the vehicle type are chosen to investigate their influence on the equivalent stress range. A two-axle truck and a six-axle truck with GVWs between 20 t and 120 t are assumed to cross the bridge at a constant speed of 15 m/s. The resulting stress histories are evaluated based on the vehicle-bridge coupled vibration system. The equivalent fatigue stresses of the bottom steel bar under various load cases are plotted in **Fig. 8**. The equivalent fatigue

stress range linearly increases with increasing GVW in association with good RRCs. In addition, the vehicle type and the RRC affect the stress range under the same GVW, where a vehicle with fewer axles or a bridge with worse RRCs produces higher stress ranges. These results demonstrate the significance of accounting for vehicle type and RRCs in the fatigue stress calculation for short-to medium-span bridges. The RRC has been emphasized by Zhang and Cai (2012) and Wang et al. (2016a; 2016b).

In addition to the vehicle type, RRC and GVW, the driving speed of a vehicle influences the VBI. Two six-axle trucks with GVWs of 40 t and 50 t are assumed to drive over a bridge with a good RRC at driving speeds between 10 m/s and 50 m/s. The equivalent stress range versus the driving speed is presented in **Fig. 9** by black solid lines. The variation trend of the equivalent stress range versus the driving speed is not monotonic, and the shapes of the two curves are different. Therefore, a linear interpolation response surface function was utilized to approximate the curves. To investigate the accuracy and efficiency of the interpolation response surface method, the driving speed intervals are assumed to be 0.1, 1, 5, and 10 m/s. The results are plotted in **Fig. 9**, where the scheme with a smaller interval value provides a better fit to the exact value (v_{int}=0.1 m/s). **Table 6** summarizes the number of intervals and the corresponding root mean square errors (RMSEs). An optimal interval speed of 1 m/s is recommended, where the number of intervals is 41, and the average RMSE is 0.0156 MPa.

Extending **Fig. 8** and **Fig. 9** to a 3D figure by considering GVW intervals of 10 t, the interpolation response surface function can be obtained, as shown in **Fig. 10**. The equivalent stress range linearly increases with an increase in GVW; however, the effect caused by the driving speed is irregular. This finding explains why a linear interpolation function instead of a

342 polynomial function was utilized to approximate the equivalent stress range.

343 These results have demonstrated the significance of the vehicle type and the RRC. In
344 addition, an interpolation response surface function was presented to approximate the
345 equivalent stress range affected by the driving speed and the GVW. For a determinate vehicle
346 type and RRC, 861 individual VBI computations were necessary for the response surface
347 function approximation. The analysis of six types of vehicles corresponds to seven hours of
348 computation by a seven-core computer. The time-consuming problem of the interpolation
349 functions can be solved by utilizing an intelligent algorithm, such as new networks and
350 learning machines, in future studies. The approximated function can replace the finite element
351 model or the time integration of **Eq. (2)**. Therefore, the subsequent stress spectrum simulation
352 based on a large number of stochastic trucks can be efficiently conducted.

353 ***Stress spectrum simulation***

354 Before conducting the fatigue stress spectrum simulation based on the stochastic traffic
355 load and the response surface functions, several realistic factors should be considered. Firstly,
356 multiple trucks may be presented simultaneously on the bridge, thereby amplifying the stress
357 range. This phenomenon leads to greater fatigue damage than that caused by a scenario with a
358 single truck (Fu et al. 2013). Secondly, since an overloaded truck is the most significant factor
359 leading to fatigue damage, reasonable traffic control with respect to truck overloading will
360 impact the stress spectrum (Cohen et al. 2003). Finally, since the fatigue is a time-relevant
361 issue, the time-variant factors should also be considered, including the RRCs and the traffic
362 growth (Wang et al. 2016b; Zhang et al. 2013).

363 A multiple presence factor (MPF) describes the scenario in which two or more trucks are

364 traveling on the bridge simultaneously (Fujino et al. 1986). In general, the MPF is a function of
365 the span length, the ADTT, and the number of lanes. In a free-flowing traffic state, the
366 probability of two trucks in a single lane is extremely low for a short-to medium-span bridge
367 with a span length of less than 40 m. The truck-by-truck analysis in a single-lane was
368 demonstrated to be conservative rather than considering a MPF (Liu et al. 2016). Therefore, the
369 present study focuses on the simultaneous presence of two trucks in neighboring lanes. Based
370 on the WIM measurements, the headway time of the trucks in two lanes was analyzed, as
371 shown in **Fig. 11**. This figure shows that 7.2% of the trucks have headway time of less than 2 s,
372 which can be treated as the threshold time for defining the simultaneous presence of two trucks
373 on the bridge. Therefore, conservatively, 7.2% of the trucks pass over the bridge in two lanes at
374 the same time.

375 To investigate the fatigue stress ranges considering the effects of multiple trucks, two
376 550-kN (GVW) six-axle trucks were used to load the bridge. The equivalent stress ranges of
377 each girder under three loading scenarios are shown in **Fig. 12**. The double-lane scenario leads
378 to a considerable increase in the stress range. The fatigue damage factor between the
379 multiple-truck and the single-truck scenarios are 3.95, 6.92 and 13.05 for the #1, #2 and #3
380 girders, respectively, as shown in **Fig. 12**. Therefore, any estimate that does not consider the
381 simultaneous presence of multiple trucks on the bridge is non-conservative. The #2 girder is
382 selected herein to conduct the stress spectrum simulation.

383 Based on the approximated response functions, 100-day stochastic traffic data were used
384 to simulate the fatigue stress spectra. Each individual truck load was inputted into the
385 corresponding response surface function, as shown in **Fig. 10**. Subsequently, 7.2% of the entire

386 truck samples were superposed randomly as a pair to consider the multiple trucks passing on
387 the bridge. To analyze the influence of traffic restrictions on the probability density of fatigue
388 stress range, the specified weights (W_s) corresponding to V2-V6 trucks with values of 20 t, 30 t,
389 40 t, 50 t and 55, respectively, are defined as the overload thresholds, in accordance with the
390 ministry of Communications and Transportation (MOCAT 2004) in China. These deterministic
391 values were used as a measurement standard to describe the overload degree of the actual
392 weights (W_a). When vehicle weights extracted from the stochastic traffic flow exceed the
393 specified overload-threshold ratio R_o ($R_o = \frac{W_a - W_s}{W_s}$), the vehicles were excluded as a comparison.
394 **Fig. 13** shows the comparison between the simulated histograms and the fittings for
395 consideration of the passage of multiple trucks and the overload limit.

396 The following conclusions have been reached based on **Fig. 13**. Firstly, the Gaussian
397 Mixture Model (GMM) adequately fits the histograms, and the multimodal features of the
398 stress spectra due to the overloaded trucks are captured by the GMM. Secondly, consideration
399 of the multiple-truck presence on the bridge leads to a slight increase in higher stress cycles
400 and a slight decrease in lower stress cycles, which are reflected in the GMM curves shown in
401 **Fig. 13(a)**. Thirdly, the truck overloading limit has a significant influence on the higher stress
402 cycles, weakening the second peak value of the GMM in **Fig. 13(b)**. These phenomena shown
403 in the stress spectra have verified the feasibility of the proposed framework for fatigue stress
404 spectrum simulation, where the simulated stress spectrum provides a reliable foundation for the
405 subsequent fatigue reliability evaluation.

Fatigue reliability evaluation

Statistics of random variables

Five random variables are included in the LSF in **Eq. (7)**: the critical fatigue damage, the fatigue strength coefficient, the distribution coefficient of transverse axle loads, the stress range and the number of stress cycles. Probabilistic models of the stress spectrum were created, as shown in **Fig. 13**. The probability model of the number of stress cycles can be fitted according to the daily traffic volume recorded by the WIM system. The remaining three random variables are discussed in the previously mentioned studies. First, in term of resistance, the critical damage accumulation index (D_{Δ}) follows a lognormal distribution with a mean value and standard deviation of 1 and 0.3, respectively (Wirsching 1984). The fatigue strength coefficient (K_D) follows a lognormal distribution with a mean value and standard deviation of 1.64×10^{14} and 0.56×10^{13}, respectively. The distribution coefficient of the transverse axle load in a traffic line follows a normal distribution with the mean value and standard deviation of 0.78 and 0.078, respectively (Lu et al. 2016). The statistics of these random variables are summarized in **Table 5**.

Fatigue reliability evaluation accounting for RRC deterioration

Since a worse RRC leads to more stress cycles and higher stress ranges, the RRC deterioration will impact the fatigue reliability of short-to medium-bridges. **Fig. 14** plots the road roughness coefficient accounting for vehicle-induced road surface deterioration according to Wang et al. (2016a). The rapid deterioration of the RRCs shown in **Fig. 14** further verifies the necessity of considering the vehicle-bridge coupled vibration in fatigue reliability

evaluation. Consider two schemes of changing the bridge decking system at 10-year intervals and at 20-year intervals. The road roughness coefficient was taken as a constant for each RRC. Based on the deterioration curve and the two repair schemes for the bridge deck system, the fatigue reliability of the bridge was evaluated via an MCS, as shown in **Fig. 15**.

In **Fig. 15,** the RRC deterioration caused a distinct decrease in reliability index. In detail, as the RRC deteriorates from "Good" to "Poor", the reliability index decreases from 2.93 to 2.47 in the 100th year. In addition, a longer repair interval will lead to lower fatigue reliability index for the bridge. Therefore, a reasonable repair scheme improves the bridge fatigue safety.

Fatigue reliability evaluation accounting for traffic growth and overload control

In addition to the RRC deterioration, the traffic load on the bridge will change over the lifetime of a bridge. The traffic growth ratio in European countries was reported approximately 2% from 2003 to 2008 (Capros et al. 2008). Considering the traffic volume increase of R_{ADTT} = 1%, 2% and 3% and a good RRC, the evaluated fatigue reliability indices are shown in **Fig. 16**. The traffic growth results in large difference in the reliability index over the service period.

The evaluated fatigue reliability can be used to predict the fatigue life of the bridge for a given target reliability index β_{target}. However, no standard value exists for β_{target} for bridge fatigue reliability evaluations. Helmerich et al. (2007) calibrated the reliability index according to ECCS 2004 and defined the β_{target} as ranging from 2.0 to 3.5. For engineering applications, Yazidani and Albrecht (1987) used 2.0 as the target reliability index when evaluating the reliability of a steel bridge. Teng and Zhao (1986) primarily studied railroad bridges in China and concluded that the fatigue reliability index of construction details in railroad bridges ranges from 1.5 to 3.6. Therefore, a value of β_{target}=2.0 was adopted in the present study to predict the

fatigue life of a bridge under the current traffic loading. Based on the target reliability index β_{target}=2.0, the fatigue life of the bridge is 260, 143, 116, and 92 years for R_{ADTT} value of 0%, 1%, 2% and 3%, respectively. Therefore, R_{ADTT} = 3% is a critical condition that might pose a threat to the fatigue reliability of the bridge.

As observed from **Fig. 13(b)**, truck overloading is the main factor that generates high stress ranges in the stress spectrum. In practice, the maximum overload ratio of the overloaded trucks recorded in the WIM is nearly 200%, and the proportion of the overloaded trucks is more than half, as observed from **Fig. 4**. Therefore, the influence of overloading control on the fatigue reliability should be investigated. Based on the simulation process of the stress spectrum shown in **Fig. 13**, the fatigue reliability of the bridge was evaluated by considering RRC=Good and R_{ADTT}=3%. The lifetime fatigue reliability accounting for traffic management is shown in **Fig. 17**.

As observed from **Fig. 17**, the fatigue reliability increases with a more rigorous overloading control measures. When R_o was assumed to be 100% and 50%, respectively, the fatigue reliability index of the bridge in lifetime increased from 1.98 to 2.21 and to 2.44, respectively. Alternatively, under the objective reliability index β =2.0, the fatigue life of the bridge increased from 92 to 127 and to 175 years, respectively. These numerical results provide an effective database for evaluating the fatigue reliability and predicting the fatigue life of a bridge subject to varying traffic loads. Based on the results, similar assessments can be performed by]bridge and traffic managers to ensure the fatigue safety of existing bridges.

Conclusions

This study presented a framework for estimating the fatigue reliability of short-to medium-

span bridges under stochastic and dynamic traffic loads. The dynamic effects of vehicle were considered in a vehicle-bridge coupled vibration system, and stochastic traffic loads were simulated based on bridge WIM measurements. To improve the effectiveness of the stress spectrum simulations, interpolation response functions were utilized to approximate the equivalent stress ranges affected by the RRCs, the driving speeds, the vehicle configurations, the GVWs and the multiple vehicle effects. The conclusions are summarized as follows:

(1) Due to the VBI, the dynamic equivalent fatigue stress range is higher than the static equivalent fatigue stress range. For a 40-m-span T-girder PC bridge with poor RRC, the fatigue damage is 1.44 times greater than the static result multiplied by the DAF. Actual assessment of bridge RRCs are essential to the implementation of the VBI system for an accurate estimation of the vehicle-induced fatigue damage in short-to medium-span bridges.

(2) The efficiency and accuracy of the response surface function are dependent on the number of intervals of both the GVW and the driving speed. Because the influence of the driving speed on the equivalent stress range is not monotonic, an interval driving speed of 1 m/s is recommended for choosing training samples to approximate the response surface function.

(3) Both RRC deterioration and traffic growth cause rapid decreases in the fatigue reliability. Therefore, the numerical results can provide a basis for a reasonable and optimal schemes for pavement repair and traffic volume control.

(4) The control of overloading has a considerable influence on the probability density of high-amplitude stresses in the fatigue stress spectrum. Even a relatively high overload limit value results in a considerable increase in the fatigue reliability of a bridge.

Further developments will improve the presented framework in the following respects. An expansion of the cumulative damage model that considers the influence of the action sequence of variable-amplitude loadings on bridge damage seems useful. Additional attention should be paid to the traffic growth model to improve predictions based on long-term monitoring data. The influence of concrete cracking, friction and slip between rebars and the concrete, and reinforcement corrosion on fatigue damage will be considered in future studies. Finally, the traffic load model and the framework will be applied to fatigue stress spectrum evaluation of welded joints in typical joints in typical short to medium span steel bridges.

Acknowledgements

The research was supported by the National Basic Research Program (973 program) of China (Grant No. 2015CB057706); the National Natural Science Foundation of China (Grant No. 51108046 and No. 51678068); the Open Fund of National Joint Engineering Research Laboratory for Long-term Performance Improvement Technology for Bridges in Southern China (Grant No. 16BCX02); the Graduate student research innovation project in Hunan province (Grant No. CX2017B460). The opinions, findings, and conclusions expressed in this study are those of the authors and do not necessarily represent the views of the sponsors.

References

AASHTO. (2012). *AASHTO LRFD bridge design specifications*, 6th Ed., Washington DC.

BSI (British Standards Institution). (2006). “Steel, concrete and composite bridges. 2: Specifications for loads.” *BS 5400*, London.

Capros, P., Mantzos, L., Papandreou, V., and Tasios, N. (2008). “European energy and

514 transport–trends to 2030–update 2007." *European Commission–Directorate-General for*
515 *Energy and Transport*, Brussels.
516 Chan, T. H., Guo, L., and Li, Z. X. (2003). "Finite element modeling for fatigue stress analysis
517 of large suspension bridges." *J. Sound. Vib.*, 261(3), 443-464.
518 Chan, T. H. T., Li, Z. X.，Ko, J. M. (2001). "Fatigue analysis and life prediction of bridges with
519 structural health monitoring data-Part Ⅱ: application." *Int. J. Fatigue*, 23(1): 55-64.
520 Chatterjee, P., Obrien, E., Li, Y., and González, A. (2006). "Wavelet domain analysis for
521 identification of vehicle axles from bridge measurements." *Comput. Struct.*, 84(28),
522 1792-1801.
523 Chen, W. Z., Xu, J., Yan, B. C., and Wang, Z. P. (2015). "Fatigue load model for highway
524 bridges in heavily loaded areas of China." *Adv. Steel Constr.*, 11(3), 322-333.
525 Chen, Z., Xu, Y., and Wang, X. (2012). "SHMS-Based Fatigue Reliability Analysis of
526 Multiloading Suspension Bridges." *J. Struct. Eng.*,
527 10.1061/(ASCE)ST.1943-541X.0000460, 299-307.
528 Cohen, H., Fu, G., Dekelbab, W., and Moses, F. (2003). "Predicting truck load spectra under
529 weight limit changes and its application to steel bridge fatigue assessment." *J.Bridge Eng.*,
530 10.1061/(ASCE)1084-0702(2003)8:5(312), 150-168.
531 Deng, L., and Cai, C. S. (2010a). "Development of dynamic impact factor for performance
532 evaluation of existing multi-girder concrete bridges." *Eng. Struct.*, 32(1), 21-31.
533 Deng, Y., Liu, Y., Feng, D. M., and Li, A. Q. (2015). "Investigation of fatigue performance of
534 welded details in long‐span steel bridges using long‐term monitoring strain data."
535 *Struct. Control Hlth.*, 22(11), 1343-1358.

536 ECS (European Committee for Standardization). (2005). “Eurocode 3: Design of steel structure
537 – Part 1-9: Fatigue.” *EN1993-1-9*, Beussels, Belgium.
538 Fu, G., Liu, L., and Bowman, M. D. (2013). “Multiple presence factor for truck load on
539 highway bridges.” *J. Bridge Eng.*, 10.1061/(ASCE)BE.1943-5592.0000330.
540 Fujino, Y., Bhartia, B. K., and Ito, M. (1986). “A stochastic study on effect of multiple truck
541 presence on fatigue damage of highway bridges.” *Struct. Eng. /Earthq. Eng.*, 3(2),
542 457-467.
543 Guo, T., Frangopol, D. M., and Chen, Y. (2012). “Fatigue reliability assessment of steel bridge
544 details integrating weigh-in-motion data and probabilistic finite element analysis.”
545 *Comput. Struct.*, 112, 245-257.
546 Han, W., Wu, J., Cai, C., and Chen, S. (2014). “Characteristics and Dynamic Impact of
547 Overloaded Extra Heavy Trucks on Typical Highway Bridges.” *J. Bridge Eng.*,
548 10.1061/(ASCE)BE.1943-5592.0000666, 05014011.
549 Lee, H. H., Jeon, J. C., and Kyung, K. S. (2012). “Determination of a reasonable impact factor
550 for fatigue investigation of simple steel plate girder railway bridges.” *Eng. Struct.*, 36,
551 316–324.
552 Liu, M., Frangopol, D. M., and Kwon, K. (2010). “Fatigue reliability assessment of retrofitted
553 steel bridges integrating monitored data.” *Struct. Saf.*, 32(1), 77-89.
554 Liu, Y., Deng, Y., and Cai, C. S. (2015). “Deflection monitoring and assessment for a
555 suspension bridge using a connected pipe system: a case study in China.” *Struct. Control
556 and Hlth.*, 22(12), 1408-1425.
557 Liu Y, Zhang H., Deng Y., Jiang N. (2016). “Effect of live load on simply supported bridges

558 under a random traffic flow based on weigh-in-motion data." *Adv. Struct. Eng*.,
559 10.1177/1369433216664348.
560 Lu, N., Noori, M., and Liu, Y. (2016). "Fatigue Reliability Assessment of Welded Steel Bridge
561 Decks under Stochastic Truck Loads via Machine Learning." *J. Bridge Eng.*,
562 10.1061/(ASCE)BE.1943-5592.0000982 , 04016105.
563 Lu, N., Liu, Y., and Noori, M. (2017). "First-passage probability of the deflection of a
564 cable-stayed bridge under long-term site-specific traffic loading." *Adv. Mech. Eng*.
565 10.1177/1687814016687271.
566 Mei, G., Qin, Q., and Lin, D. J. (2004). "Bimodal renewal processes models of highway
567 vehicle loads." *Reliab. Eng. Syst. Safe.*, 83(3), 333-339.
568 Miner, M. A. (1945). "Cumulative damage in fatigue." *J. Appl. Mech.*, 12(3), 159-164.
569 MOCAT (Ministry of Communications and Transportation). (2015). "General code for design
570 of highway bridges and culverts." *JTG D60-2015*, Beijing, China.
571 MOCAT (Ministry of Communications and Transportation). (2004) "Limits of dimensions,
572 axle load and masses for road vehicles." *GB 1589-2004*, Beingjing, China.
573 Mohammadi, J. and Polepeddi, R. (2000). "Bridge rating with consideration for fatigue damage
574 from overloads." *J. Bridge Eng*., 10.1061/(ASCE)1084-0702(2000)5:3(259), 259-265.
575 OBrien, E. and Enright, B. (2013). "Using weigh-in-motion data to determine aggressiveness
576 of traffic for bridge loading." *J. Bridge Eng.*, 10.1061/(ASCE)BE.1943-5592.0000368,
577 232-239.
578 Pais, J., Amorim, S., and Minhoto, M. (2013). "Impact of traffic overload on road pavement
579 pserformance." *J. Transp. Eng.*, 10.1061/(ASCE)TE.1943-5436.0000571, 873-879.

580 Rosemarie H, Bertram Kühn, and Alain Nussbaumer. (2007). "Assessment of existing steel
581 structures. a guideline for estimation of the remaining fatigue life." *Struct. Infrastruct. E.*
582 3(3), 245-255.
583 Soliman, M., Barone, G., and Frangopol, D. M. (2015). "Fatigue reliability and service life
584 prediction of aluminum naval ship details based on monitoring data." *Struct. Health*
585 *Monit.*, 14(1), 3-19.
586 Teng Z B and Zhao Y. K. (1986). "Fatigue reliability of railway bridges in China." *Proce. of*
587 *IABSE Symposium*, Tokyo.
588 Wang, C. S., Yen, B. T., Li, H. T., and Duan, L. (2015). "Fatigue life evaluation of in-service
589 steel bridges by using bi-linear s-n curves." *Adv. Steel Constr.*, 11(3), 269-282.
590 Wang, T., Liu, C., Huang, D., and Shahawy, M. (2005). "Truck loading and fatigue damage
591 analysis for girder bridges based on weigh-in-Motion data." *J. Bridge Eng.*,
592 10.1061/(ASCE)1084-0702(2005)10:1(12), 12-20.
593 Wang, W. and Deng, L. (2015). "Impact factors for fatigue design of steel I-girder bridges
594 considering the deterioration of road surface condition." *J. Bridge Eng.*,
595 10.1061/(ASCE)BE.1943-5592.0000885, 04016011.
596 Wang, W., Deng, L., and Shao, X. (2016a). "Number of stress cycles for fatigue design of
597 simply-supported steel I-girder bridges considering the dynamic effect of vehicle loading."
598 *Eng. Struct.*, 110, 70-78.
599 Wang, W., Deng, L., and Shao, X. (2016b). "Fatigue design of steel bridges considering the
600 effect of dynamic vehicle loading and overloaded trucks." *J. Bridge Eng.*,
601 10.1061/(ASCE)BE.1943-5592.0000914, 04016048.

602 Wirsching, P. (1984). “Fatigue reliability for offshore structures.” *J. Struct. Eng.*,
603 10.1061/(ASCE)0733-9445(1984)110:10(2340), 2340-2356.
604 Yazdani, N., and Albrecht, P. (1987). “Risk analysis of fatigue failure of highway steel bridges.”
605 *J. Struct. Eng.*, 10.1061/(ASCE)0733-9445(1987)113:3(483),483-500.
606 Zhang, W. and Cai, C. (2012). “Fatigue Reliability Assessment for Existing Bridges
607 Considering Vehicle Speed and Road Surface Conditions.” *J. Bridge Eng*.,
608 10.1061/(ASCE)BE.1943-5592.0000272, 443-453.
609 Zhang, W., Cai, C. S., and Pan, F. (2013). “Nonlinear fatigue damage assessment of existing
610 bridges considering progressively deteriorated road conditions.” *Eng. Struct.*, 56(56),
611 1922-1932.
612

▪ Tables Captions

Table 1. Parameters of the S-N curves in Eurocode3 for a steel bar

Table 2. Physical properties of the bridge examples

Table 3. Comparisons of the DAFs and the fatigue damage ratio

Table 4. Influence of interval length on the accuracy and efficiency of the interpolation response surface method

Table 5. Parameters in the GMMs of the stress spectra

Table 6. Statistics of random variables

622 **Table 1.** Parameters of the S-N curves in Eurocode3 for steel bar

Classification	$\Delta\sigma_C$(MPa)	$\Delta\sigma_D$ (MPa)	$\Delta\sigma_L$ (MPa)	K_C	K_D
Steel bar	80	59	32	1.02×10^{12}	1.64×10^{14}

623
624

625 **Table 2.** Physical properties of the bridge examples

L_b(m)	H_b(m)	A_c(m^2)	A_s(m^2)	E(Pa)	I(m^4)	y(m)
20	1.7	0.9820	6.15×10^{-4}	1.95×10^{11}	0.2922	1.2098
40	2.5	1.139	6.15×10^{-4}	1.95×10^{11}	0.7950	1.6079

626
627

628 **Table 3.** Comparisons of the DAFs and the fatigue damage ratio

Bridge length	L = 25 m		L = 40 m	
RRC	Good	Poor	Good	Poor
DAF_{code}	1.27		1.19	
DAF of $\Delta\sigma_{re}$	1.15	1.44	1.12	1.28
Fatigue damage ratio	0.61	1.87	0.74	1.44

629
630

631 **Table 4.** Influence of interval length on the accuracy and efficiency of the interpolation
632 response surface method

Interval speed (m/s)	$v_{int} = 0.1$	$v_{int} = 1$	$v_{int} = 5$	$v_{int} = 10$
Number of intervals	401	41	9	5
RMSE for GVW=40 t (MPa)	0	0.0156	0.1352	0.5516
RMSE for GVW=50 t (MPa)	0	0.0161	0.1417	0.4890

633
634

635 **Table 5.** Parameters in the GMMs of the stress spectra

Case	w_1	μ_1 (MPa)	σ_1 (MPa)	w_2	μ_2 (MPa)	σ_2 (MPa)
P_m=0, R_o=non	0.56	6.97	2.23	0.44	15.02	4.85
p_m=7.2%, R_o=non	0.51	6.96	2.33	0.49	14.84	5.73
P_m=7.2%, R_o=100%	0.51	6.76	2.75	0.49	13.77	5.55
P_m=7.2, R_o=50%	0.68	6.42	3.95	0.32	12.97	5.23

636

637

638 **Table 6.** Statistics of random variables

Variable	Distribution type	Mean value	Standard deviation
$\Delta\sigma_{re}$	GMM	Figs. 11	
N_d	Normal distribution	1072	161
D_{Δ}	Lognormal distribution	1	0.3
K_D	Lognormal distribution	1.64×10^{14}	0.56×10^{13}
e	Normal distribution	0.78	0.078

639

640

▪ Figures Captions

Fig. 1. Physical model of a two-axle truck

Fig. 2. Flowchart for simulating fatigue stress spectrum based on WIM data

Fig. 3. Statistics of WIM measurements: (a) GVWs of V6 trucks; (b) driving speeds of V6 trucks

Fig. 4. Stochastic traffic load model over one hour

Fig. 5. Dimensions of the cross-section of (b) the mid-span of the bridge; and (b) a typical girder (unit: m)

Fig. 6. Time histories of the simulated road roughness coefficients

Fig. 7. Stress-time histories of the bottom rebar of the bridge under a V6 truck loading: (a) L_b = 25 m; (b) L_b = 40 m

Fig. 8. Influence of vehicle types and GVWs on equivalent fatigue stress ranges

Fig. 9. Influence of driving speeds on the equivalent stress range

Fig. 10. Response surface of fatigue stress ranges for six-axle trucks driving on good RRC considering driving speeds and GVWs

Fig. 11. Histograms of the headway time of two trucks passing over the bridge simultaneously in two lanes

Fig. 12. Influence of travel lanes on stress ranges

Fig. 13. Stress spectra and GMM fits of the bridge (a) considering the presence of mutiple trucks; and (b) considering overloading control

Fig. 14. RRC deterioration due to vehicle loads

Fig. 15. Lifetime reliability accounting for RRC degradation

663 **Fig. 16.** Lifetime fatigue reliability of the bridge considering traffic growth

664 **Fig. 17.** Influence of truck overloading limits on the fatigue reliability

Fig. 1. Physical model of a two-axle truck

Click here to download Figure Fig 1.pdf

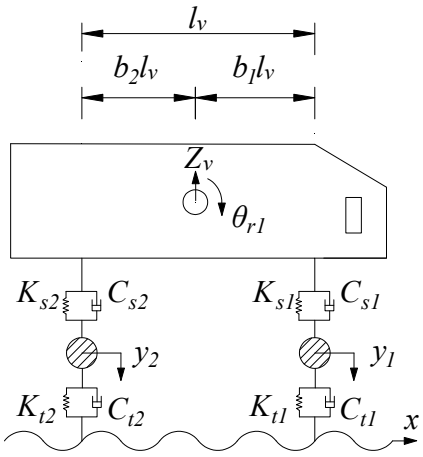

Fig. 2. Flowchart for simulating fatigue stress spectrum based on WIM data

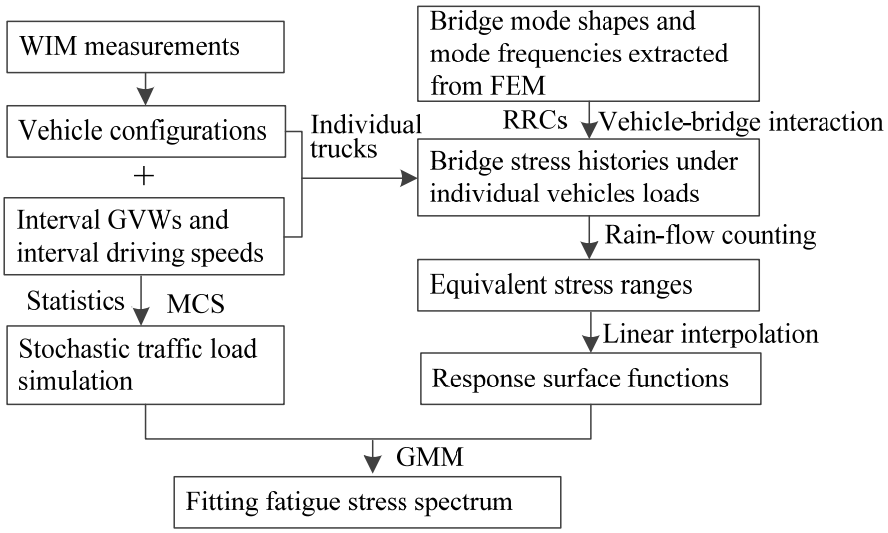

Fig. 3. Statistics of WIM measurements: (a) GVWs of V6 trucks; (b) driving speeds of V6 trucks

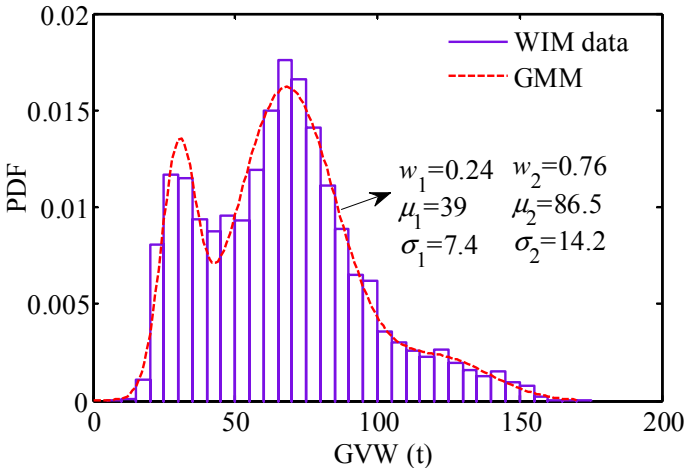

(a)

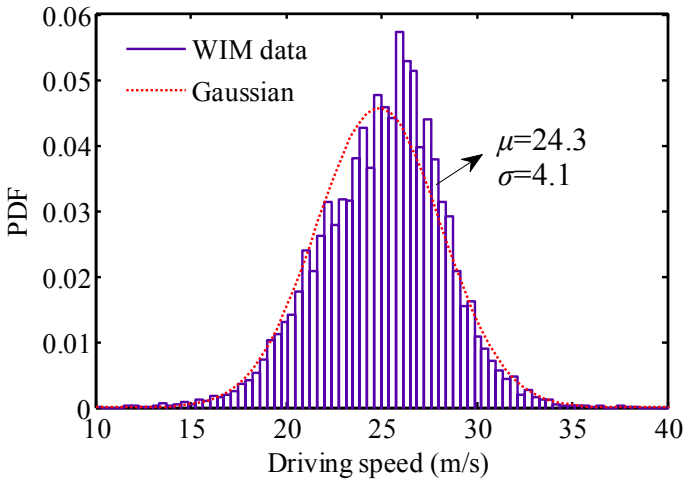

(b)

Fig. 4. Stochastic traffic load model over one hour

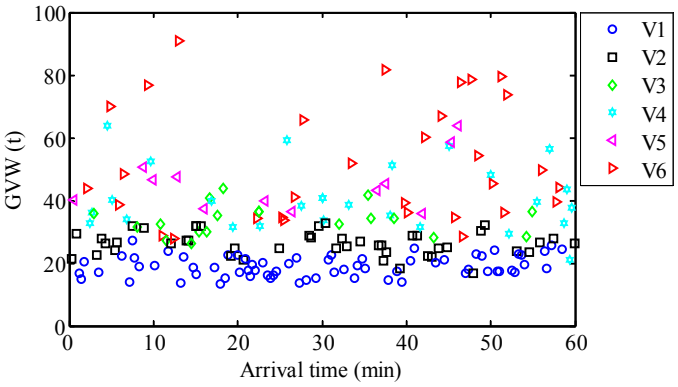

Fig 5. Dimensions of the cross-section of (b) the mid-span of the bridge; and (b) a typical girder (unit: m)

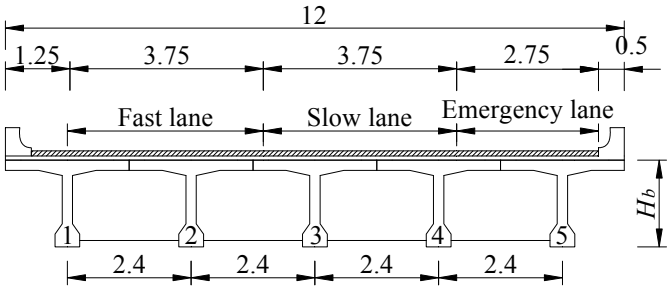

(a)

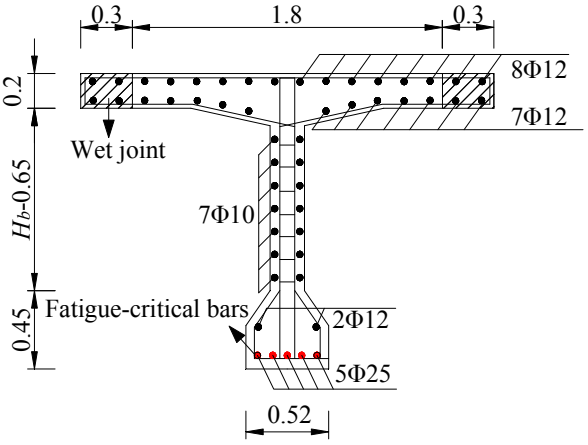

(b)

Fig. 6. Time histories of the simulated road roughness coefficients

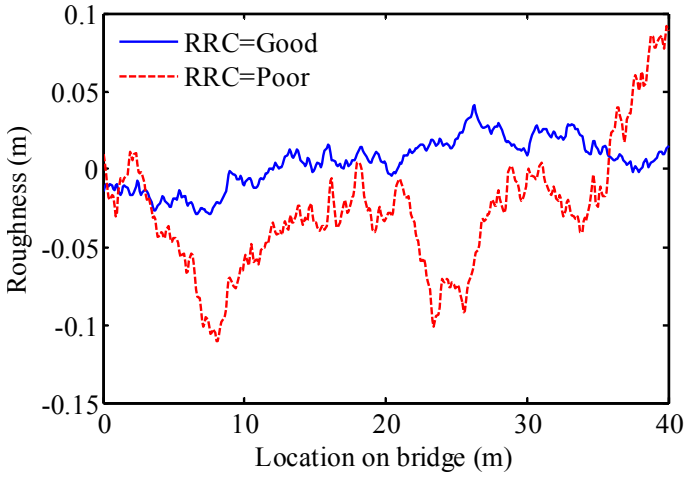

Fig. 7. Stress-time histories of the bottom rebar of the bridge under a V6 truck loading: (a) Lb = 25 m; (b) Lb = 40 m

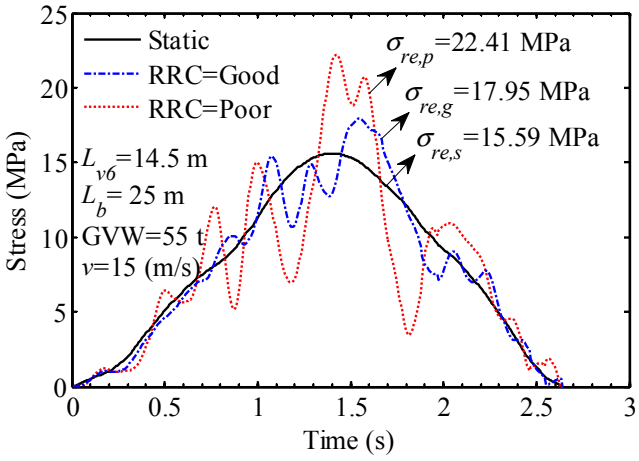

(a)

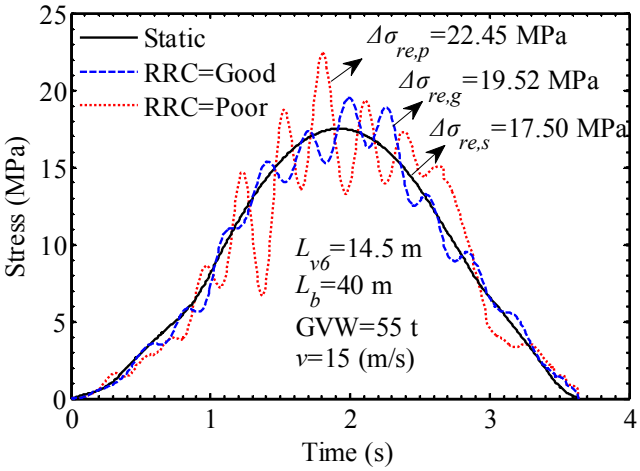

(b)

Fig. 8. Influence of vehicle types and GVWs on equivalent fatigue stress ranges

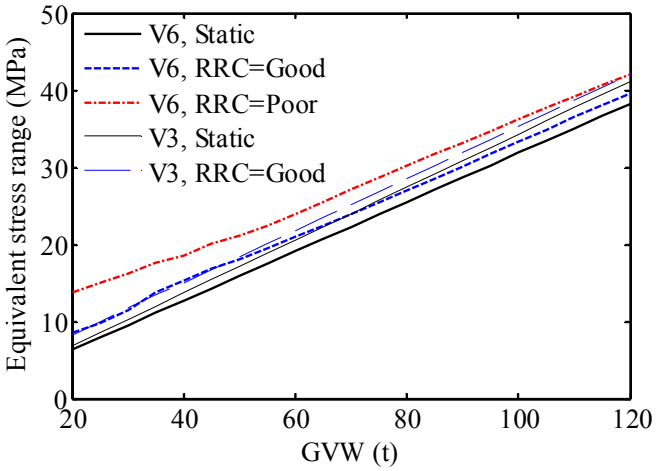

Fig. 9. Influence of driving speeds on the equivalent stress range

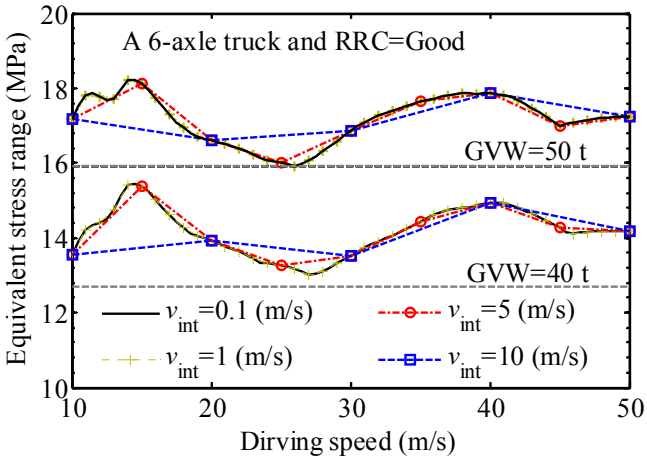

Fig. 10. Response surface of fatigue stress ranges for six-axle trucks driving on good RRC considering driving speeds and

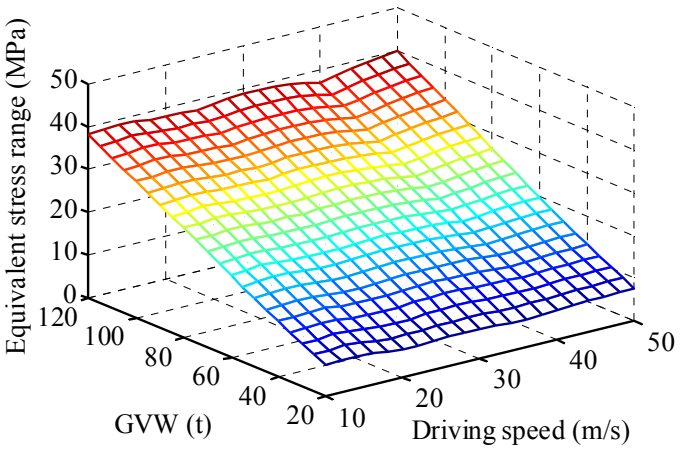

Fig. 11. Histograms of the headway time of two trucks passing over the bridge simultaneously in two lanes

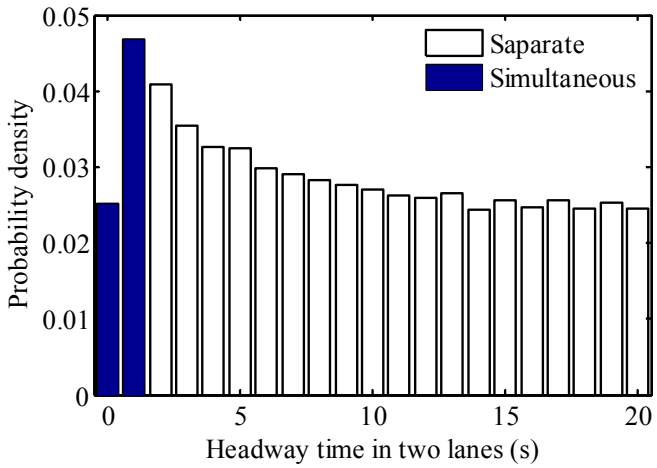

Fig. 12. Influence of travel lanes on stress ranges

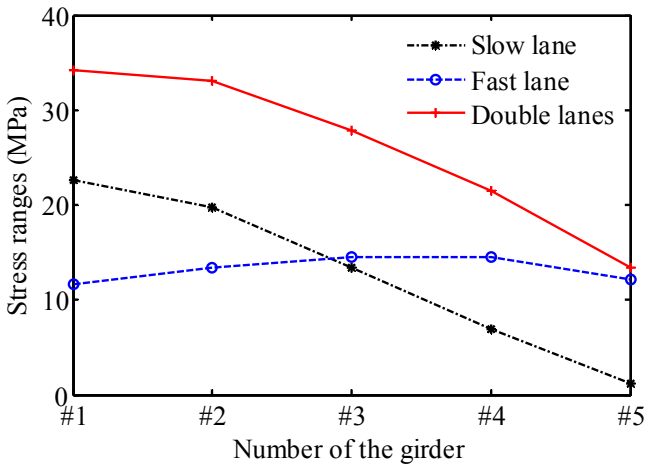

Fig. 13. Stress spectra and GMM fits of the bridge (a) considering the presence of mutiple trucks; and (b) considering

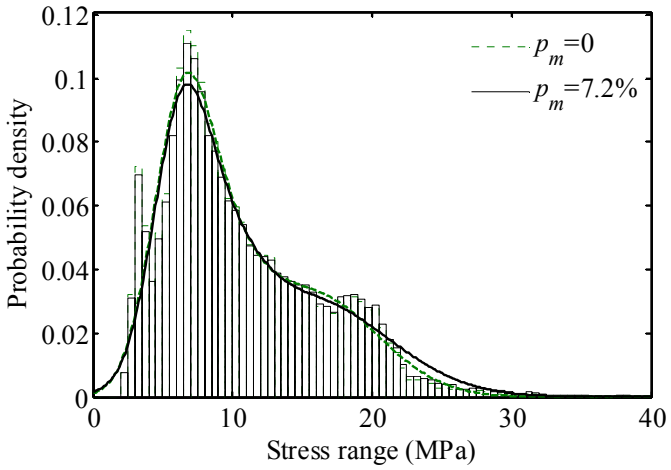

(a)

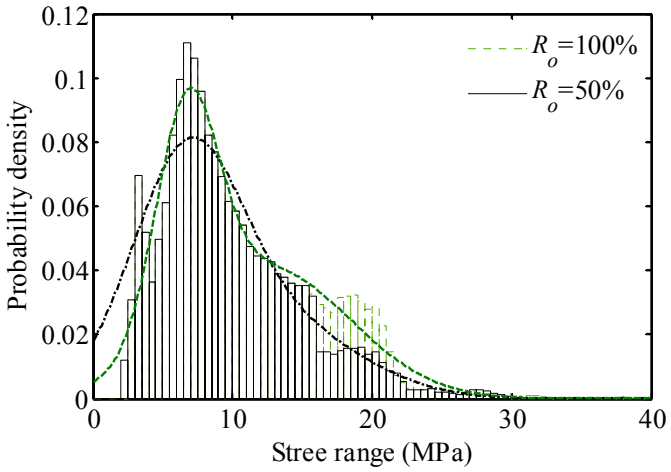

(b)

Fig. 14. RRC deterioration due to vehicle loads

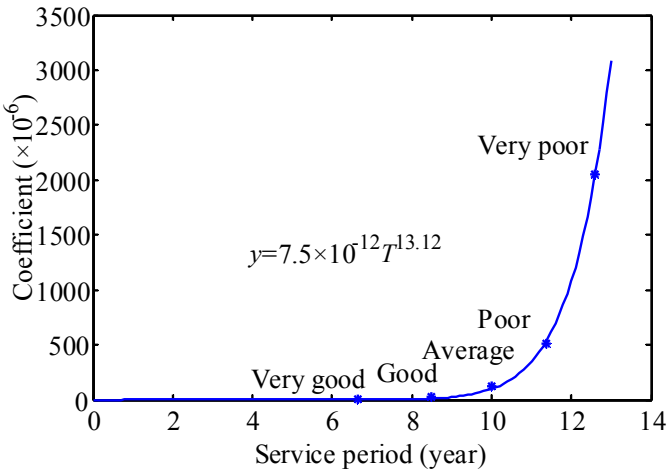

Fig. 15. Lifetime reliability accounting for RRC degradation

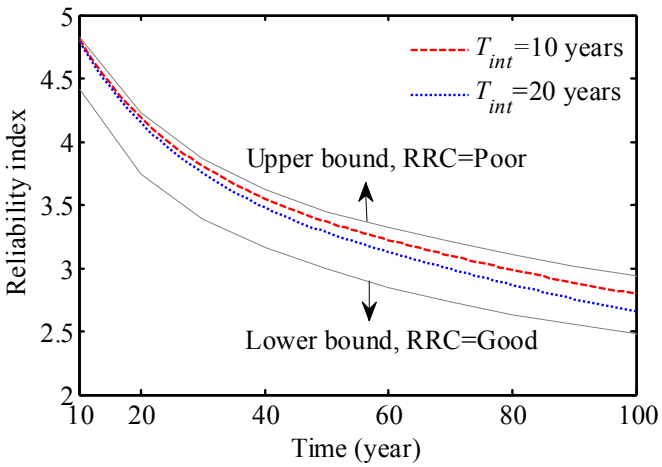

Fig. 16. Lifetime fatigue reliability of the bridge considering traffic growth

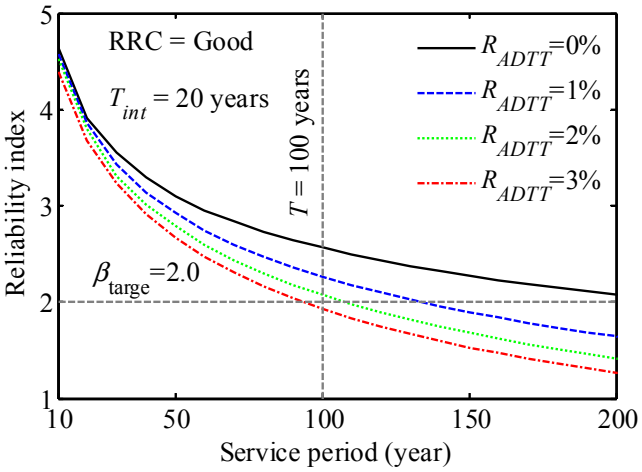

Fig. 17. Influence of truck overloading limits on the fatigue reliability